Nonperturbative time-dependent approach to breakup of halo nuclei

V. S. Melezhik[1,2] and D. Baye[1]
[1]*Physique Nucléaire Théorique et Physique Mathématique, C.P. 229, Université Libre de Bruxelles, B-1050 Brussels, Belgium*
[2]*Joint Institute for Nuclear Research, Dubna, Moscow Region 141980, Russian Federation*
(Received 29 December 1998)

The time-dependent mesh method is proposed as an efficient tool for a quantitative analysis of the Coulomb breakup of halo nuclei. The approach allows a treatment of breakup reactions in the nonperturbative regime. It avoids any multipole expansion for the Coulomb interaction between the projectile and the target. Moreover, it permits using more general trajectories allowing an estimation of postacceleration effects. This numerical technique is applied to the $^{11}\mathrm{Be}+^{208}\mathrm{Pb}\rightarrow{}^{10}\mathrm{Be}+n+^{208}\mathrm{Pb}$ breakup reaction at 72 MeV per nucleon and is compared with experiment and with a previous calculation. Corrections due to the projectile deflection from a straight-line trajectory and to the neutron spin rotation are found to be weak for the specific collision parameters. [S0556-2813(99)00306-4]

PACS number(s): 25.60.Gc, 25.70.De, 02.70.Jn, 27.20.+n

I. INTRODUCTION

Coulomb breakup is one of the main tools for the study of halo nuclei [1]. The breakup cross section provides useful information about the structure of the halo. Therefore, this topic is the subject of intensive experimental and theoretical investigations. Among halo nuclei, the ^{11}Be nucleus is of particular importance because the relative simplicity of its structure allows more accurate theoretical investigations. Indeed, its two bound states can be fairly well described as a ^{10}Be core to which a neutron is loosely bound. With a good approximation, the breakup can be seen as a transition from a two-particle bound state to the continuum, due to a varying Coulomb field.

Recently, efficient mesh methods [2–4] of solution of the time-dependent Schrödinger equation have been developed for quantitatively treating the time evolution of the projectile-nucleus wave function in this kind of reaction. These analyses were performed with three spatial dimensions for the relative motion of the halo neutron with respect to the core. From a physical viewpoint, they are attractive owing to the simplicity of the treatment of time dependence. However some simplifications in these computations, i.e., the use of a multipole expansion for the Coulomb field between the halo nucleus and the target and the application of a perturbation approximation in the computation of the total breakup cross sections, may introduce significant limitations in further developments of this approach.

In the present work, the time-dependent Schrödinger equation is solved with a nonperturbative algorithm on a three-dimensional spatial mesh which does not suffer from the abovementioned limitations. In fact, the method allows much flexibility in the definition of the trajectory of the projectile. Different effects can be taken into account such as the Coulomb repulsion between the target and projectile or spin coupling effects. The method [5–7] makes use of values of the wave function at mesh points in angular space, in the spirit of the discrete-variable or Lagrange-mesh methods (see Ref. [8], and references therein). The radial functions are approximated with variable-step finite-difference techniques. The splitting-up method [9] accurately describes the time evolution of the system. The efficiency of the present approach is illustrated by studying the Coulomb breakup reaction $^{11}\mathrm{Be}+^{208}\mathrm{Pb}\rightarrow{}^{10}\mathrm{Be}+n+^{208}\mathrm{Pb}$ at an energy (72 MeV per nucleon) where experimental data are available [10] and where another mesh method has recently been applied [4].

In Sec. II, the physical problem is recalled and modelized. The computational algorithm is described. In Sec. III, the conditions of the calculation are discussed and compared with those of Ref. [4]. The convergence of the method is analyzed in Sec. IV. The obtained results are discussed in Sec. V. The last section is devoted to concluding remarks.

II. THEORETICAL FRAMEWORK

A. Model

The ^{10}Be core nucleus is treated as a structureless particle which is weakly bound to the halo neutron by the potential $V(\boldsymbol{r})$, where $\boldsymbol{r}$ is the coordinate between the core nucleus and the neutron. In such an approach, the reaction $^{11}\mathrm{Be}+^{208}\mathrm{Pb}\rightarrow{}^{10}\mathrm{Be}+n+^{208}\mathrm{Pb}$ in the projectile rest frame follows the time-dependent Schrödinger equation

$$i\hbar\frac{\partial}{\partial t}\Psi(\boldsymbol{r},t)=H(\boldsymbol{r},t)\,\Psi(\boldsymbol{r},t)=[H_0(\boldsymbol{r})+h(\boldsymbol{r},t)]\,\Psi(\boldsymbol{r},t), \tag{1}$$

where the wave packet $\Psi(\boldsymbol{r},t)$ describes the relative motion of the neutron and the core. In this expression

$$H_0=-\frac{\hbar^2}{2\mu}\triangle_{\boldsymbol{r}}+V(\boldsymbol{r}) \tag{2}$$

is the ^{11}Be internal Hamiltonian with reduced mass $\mu=m_n m_c/M$, where m_n, m_c and $M=m_n+m_c$ are the neutron, ^{10}Be-core, and ^{11}Be masses, respectively. The potential $V(\boldsymbol{r})$ is the sum of an l-dependent central potential $V_l(r)$ and a spin-orbit interaction $V_l^s(r)\,\boldsymbol{l}\cdot\boldsymbol{s}$. The interaction of the target nucleus with the projectile

$$h(\boldsymbol{r},t)=V_C(\boldsymbol{r},t)+V_{sc}(\boldsymbol{r},t) \tag{3}$$

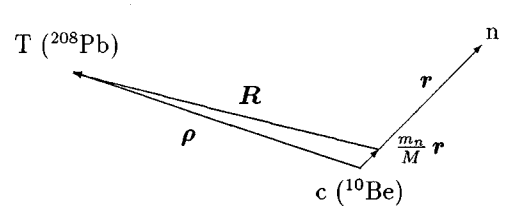

FIG. 1. Coordinates appearing in the definitions of potential V_C [Eqs. (4) and (5)].

is described by two terms in our model.

The time-dependent Coulomb potential $V_C(\boldsymbol{r},t)$ is defined in two different ways which correspond to different modelings of the reaction mechanism. The first definition reads

$$V_C(\boldsymbol{r},t)=\frac{Z_cZ_Te^2}{|m_n\boldsymbol{r}/M+\boldsymbol{R}(t)|}-\frac{Z_cZ_Te^2}{R(t)}, \tag{4}$$

where Z_c and Z_T are the charge numbers of the core and target, respectively, and $\boldsymbol{R}(t)$ is the relative coordinate between the projectile and the target (see Fig. 1). With a straight-line trajectory $\boldsymbol{R}(t)=\boldsymbol{b}+\boldsymbol{v}_0t$ where $\boldsymbol{b}$ is the impact vector and $\boldsymbol{v}_0$ is the initial velocity, this definition corresponds to previous models [2–4]. Equation (4) is also able to simulate the projectile deceleration before the collision as well as its acceleration afterwards by using a Coulomb trajectory for $\boldsymbol{R}(t)$. However, the core postacceleration due to the neutron emission is not described. In the following, we refer to approaches based on Eq. (4) as the ''bound-neutron model.''

In order to evaluate the importance of postacceleration effects, we choose the second definition

$$V_C(\boldsymbol{r},t)=\frac{Z_cZ_Te^2}{\rho(t)}-\frac{Z_cZ_Te^2}{|\boldsymbol{\rho}(t)-m_n\boldsymbol{r}/M|}, \tag{5}$$

where $\boldsymbol{\rho}(t)$ is the relative coordinate between the target and the projectile core (see Fig. 1). It corresponds to the so-called ''free particle'' mechanism discussed earlier [11] when only the core is acted upon by the target Coulomb field without influence of the neutron. The core follows its own trajectory which is not affected by a shift between the charged core location and the ^{11}Be center of mass. In the following, we refer to approaches based on Eq. (5) as the ''free-neutron model.''

In some calculations, we also introduce the interaction $V_{sc}(\boldsymbol{r},t)$ describing the coupling of the neutron spin $\boldsymbol{s}$ with the varying electric field of the target

$$V_{sc}(\boldsymbol{r},t)=-g_n\frac{Z_Te^2\hbar}{2m_nc^2}\frac{1}{|\boldsymbol{\rho}(t)-\boldsymbol{r}|^3}\,\boldsymbol{s}\cdot\boldsymbol{v}(t)\times[\boldsymbol{\rho}(t)-\boldsymbol{r}], \tag{6}$$

where g_n is the neutron gyromagnetic factor and $\boldsymbol{v}$ is the relative velocity of the projectile and the target.

B. Angular-subspace discretization

For solving the time-dependent four-dimensional Schrödinger equation (1), we apply a nonperturbative approach [7], which has been developed recently and used in a number of nonstationary problems of muon [5] and atomic [6,7] physics. We seek a solution $\Psi(\boldsymbol{r},t)$ in spherical coordinates $(r,\Omega)\equiv(r,\theta,\phi)$ as an expansion

$$\Psi(\boldsymbol{r},t)=\frac{1}{r}\sum_s\sum_{\nu j}^{N}\varphi_\nu(\Omega)(\varphi^{-1})_{\nu j}\psi_j^s(r,t) \tag{7}$$

over the two-dimensional basis

$$\varphi_\nu(\Omega)=\tilde{P}_l^m(\theta)\times\begin{cases}\cos m\phi, & m>0,\\ \dfrac{1}{\sqrt{2}}, & m=0,\\ \sin m\phi, & m<0.\end{cases} \tag{8}$$

In this basis, $\tilde{P}_l^m(\theta)$ is in general an associated Legendre polynomial $P_l^{|m|}(\theta)$, with a few possible exceptions as explained below after Eq. (9). The symbol ν represents $\{l,m\}$ where m takes $\sqrt{N}$ values varying between $\pm(\sqrt{N}-1)/2$ and l takes $\sqrt{N}$ values starting with $|m|$. The sum over ν, $\Sigma_{\nu=1}^{N}$, is equivalent to the double sum $\Sigma_{m=-(\sqrt{N}-1)/2}^{(\sqrt{N}-1)/2}\Sigma_{l=|m|}^{|m|+\sqrt{N}-1}$.

The basis (8) is associated with a mesh. For the θ variable, the $\sqrt{N}$ mesh points θ_{j_θ} are chosen from the zeros of the Legendre polynomial $P_{\sqrt{N}}(\cos\theta_{j_\theta})$. For the ϕ variable, the $\sqrt{N}$ mesh points are chosen as $\phi_{j_\phi}=\pi(2j_\phi-1)/\sqrt{N}$. The total number N of grid points $\Omega_j=(\theta_{j_\theta},\phi_{j_\phi})$ is equal to the number of basis functions in expansion (7) [6,7]. To this mesh are associated N weights λ_j which are the products of the standard Gauss-Legendre weights by $2\pi/\sqrt{N}$. The $(\varphi^{-1})_{\nu j}$ are the elements of the $N\times N$ matrix φ^{-1} inverse to the matrix with elements $\varphi_{\nu j}=\varphi_\nu(\Omega_j)$ defined at the grid points Ω_j. The polynomials $\tilde{P}_l^m(\theta)$ are chosen in such a way that one has exactly

$$\int\varphi_\nu(\Omega)\varphi_{\nu'}(\Omega)d\Omega=\sum_j\lambda_j\varphi_{\nu j}\varphi_{\nu' j}=\delta_{\nu\nu'} \tag{9}$$

for all ν and $\nu'\leqslant N$. For most ν and ν', property (9) is automatically satisfied because the basis functions $\varphi_\nu(\Omega)$ are orthogonal and the Gauss quadrature is exact. However, in a few cases with the highest l values, some polynomials $\tilde{P}_l^m$ have to be specially made orthogonal in the sense of the Gauss quadrature. With this choice, the matrix $\lambda_j^{1/2}\varphi_{\nu j}$ is orthogonal.

The radial components $\psi_j^s(r,t)$ correspond to $\psi(r,\Omega_j,t)|s\rangle$ where $|s\rangle=|\pm1/2\rangle$ is a spin state and $\psi(r,\Omega_j,t)$ is a complex function. Let us introduce the $2N$-component vector $\boldsymbol{\Psi}(r,t)=\{\lambda_j^{1/2}\psi_j^s(r,t)\}$. With respect to the unknown coefficients in expansion (7), the problem is reduced to a system of Schrödinger-type equations

$$i\hbar\frac{\partial}{\partial t}\boldsymbol{\Psi}(r,t)=[\hat{H}_0(r)+\hat{h}(r,t)]\,\boldsymbol{\Psi}(r,t). \tag{10}$$

In this system, $\hat{H}_0(r)$ and $\hat{h}(r,t)$ are $2N\times2N$ matrix operators representing H_0 and h [Eqs. (2) and (3)] on the grid. The elements of $\hat{H}_0(r)$ are defined by

$$H_{0kj}^{ss'}(r)=\left\{ -\frac{\hbar^2}{2\mu}\frac{\partial^2}{\partial r^2}\delta_{kj}+(\lambda_k\lambda_j)^{-1/2}\sum_{\nu=\{l,m\}}^{N}(\varphi^{-1})_{\nu k}\times\left[V_l^s(r)+\frac{\hbar^2}{2\mu r^2}l(l+1)\right](\varphi^{-1})_{\nu j}\right\}\delta_{ss'}, \quad (11)$$

where $V_l^s(r)$ is the diagonal matrix element of a spherical potential between the neutron and the core in the lth partial wave calculated with the spin state $|s\rangle$ [4].

The elements of $\hat{h}(r,t)$ read

$$h_{kj}^{ss'}(r,t)=[V_C(r,\Omega_k,t)\delta_{ss'}+V_{sc}^{ss'}(r,\Omega_k,t)]\delta_{kj}. \quad (12)$$

Notice that the time-dependent Coulomb operator defined in Eq. (4) or (5) is diagonal in such a representation and does not require the multipole expansion used in other approaches [2–4].

C. Computational scheme

Another attractive peculiarity of the present approach is that the only nondiagonal part of the Hamiltonian in Eq. (10) is in the block matrices $\hat{H}_0^{ss}$ [Eq. (11)]. For each spin state, they can be diagonalized by the simple unitary transform $S_{\nu k}=\lambda_k^{1/2}\varphi_{\nu k}$ [7]. This property has been exploited for developing an economic algorithm with a computational time proportional to the number N of unknowns in the system of equations (10) [7]. The splitting-up method [9] has been applied for the propagation in time $t_n\rightarrow t_{n+1}=t_n+\Delta t$ as

$$\mathbf{\Psi}(r,t_n+\Delta t)=(1+\tfrac{1}{2}i\Delta t\,\hat{h})^{-1}(1-\tfrac{1}{2}i\Delta t\,\hat{h})\times(1+\tfrac{1}{2}i\Delta t\,\hat{H}_0)^{-1}(1-\tfrac{1}{2}i\Delta t\,\hat{H}_0)\mathbf{\Psi}(r,t_n). \quad (13)$$

Thus the problem is split up into two steps involving the intermediate time $t_n+\frac{1}{2}\Delta t$.

At the initial step, the vector function $\mathbf{\Psi}(r,t_n+\frac{1}{2}\Delta t)$ is evaluated from the known vector function $\mathbf{\Psi}(r,t_n)$ with the system of N differential equations

$$[1+\tfrac{1}{2}i\Delta t\,\hat{S}\hat{H}_0(r)\hat{S}^{\dagger}]\overline{\mathbf{\Psi}}(r,t_n+\tfrac{1}{2}\Delta t)=[1-\tfrac{1}{2}i\Delta t\,\hat{S}\hat{H}_0(r)\hat{S}^{\dagger}]\overline{\mathbf{\Psi}}(r,t_n), \quad (14)$$

where

$$\overline{\mathbf{\Psi}}(r,t_n)=\hat{S}\mathbf{\Psi}(r,t_n). \quad (15)$$

The system of equations (14) is uncoupled since

$$(\hat{S}\hat{H}_0\hat{S}^{\dagger})_{\nu\nu'}^{ss'}=\left[-\frac{\hbar^2}{2\mu}\frac{\partial^2}{\partial r^2}+V_l^s(r)+\frac{\hbar^2}{2\mu r^2}l(l+1)\right]\delta_{ss'}\delta_{\nu\nu'}, \qquad \nu=\{l,m\}. \quad (16)$$

It is solved with the boundary conditions

$$\overline{\mathbf{\Psi}}(0,t_n+\tfrac{1}{2}\Delta t)=\overline{\mathbf{\Psi}}(r_m,t_n+\tfrac{1}{2}\Delta t)=0, \quad r_m\rightarrow\infty. \quad (17)$$

Then the wave function at time $t_n+\frac{1}{2}\Delta t$ is obtained as

$$\mathbf{\Psi}(r,t_n+\tfrac{1}{2}\Delta t)=\hat{S}^{\dagger}\overline{\mathbf{\Psi}}(r,t_n+\tfrac{1}{2}\Delta t). \quad (18)$$

The most time-consuming part in performing the initial step $t_n\rightarrow t_n+\frac{1}{2}\Delta t$ [Eqs. (15)–(18)], i.e., solving the boundary-value problem (14) and (17), demands only N computational operations. Moreover, the $\hat{S}$ transformation is time independent and r independent and, as a consequence, the matrix $S_{\nu k}=\lambda_k^{1/2}\varphi_{\nu}(\Omega_k)$ has to be evaluated only once.

At the second step, the system of N uncoupled algebraic equations

$$[1+\tfrac{1}{2}i\Delta t\,\hat{h}(r,t_n)]\mathbf{\Psi}(r,t_n+\Delta t)=[1-\tfrac{1}{2}i\Delta t\,\hat{h}(r,t_n)]\mathbf{\Psi}(r,t_n+\tfrac{1}{2}\Delta t) \quad (19)$$

with the matrix $\hat{h}(r,t_n)$ defined in Eq. (12) which is nondiagonal only in the spin space, is then solved. Applying the split-operator method (15)–(19) to problem (10) demands that the two-dimensional basis $\varphi_{\nu}(\Omega)$, used in Eq. (7), is orthogonal on the grid Ω_k. It is shown in Ref. [7] that, because of the simplicity of the diagonalization procedure for the $\hat{H}_0(r)$ operator, the computational time for solving problem (15)–(19) is approximately proportional to N as long as the calculation in Eq. (18) is negligible, i.e., when N is not too large.

III. CONDITIONS OF THE CALCULATION

The time evolution of the system is calculated according to the above scheme starting from the initial state $\Psi(\boldsymbol{r},T_{in})=\phi_{1s}(\boldsymbol{r})$, where $\phi_{1s}(\boldsymbol{r})$ is the ground-state wave function of the projectile Hamiltonian $H_0(\boldsymbol{r})$. Following the parametrization suggested in Ref. [4], the interaction V between the neutron and the ^{10}Be core is chosen as the sum of a spherical Woods-Saxon potential $V_l(r)=V_l f(r)$, with the radius $R_0=2.669$ fm and the diffuseness $a=0.6$ fm, and of a standard spin-orbit interaction

$$V_l^s(r)\boldsymbol{l}\cdot\boldsymbol{s}=V_{ls}\frac{1}{r}\frac{d}{dr}f(r)\boldsymbol{l}\cdot\boldsymbol{s}. \quad (20)$$

The standard value $V_{ls}=32.8$ MeV fm^2 is used for the depth of the ls potential for a p-shell nucleus [4]. The depths of the Woods-Saxon potentials have been determined as $V_0=-59.5$ MeV ($l=0$) and $V_l=-40.5$ MeV ($l\geqslant 1$) in order to locate the $1/2^+$ ground state of ^{11}Be at -0.503 MeV and the $1/2^-$ excited state at -0.183 MeV [4] with respect to the threshold for neutron breakup. Notice the considerable deviation of the V_0 value employed here for the ground state from $V_0=-58.2$ MeV used in Ref. [4]. The analysis presented below explains the reason for this variation.

For approximating Eq. (14) with respect to the radial variable r, a second-order finite-difference approximation on a quasiuniform grid has been used on the interval $r\in[0,r_m]$ with $r_m=800$ fm in this section as in Ref. [4]. The grid has been realized by the mapping $r\rightarrow x$ of the initial interval onto $x\in[0,1]$ by the formula $r=r_m(e^{8x}-1)/(e^8-1)$ [6]. Table I illustrates the convergence of the scheme as $\Delta r\rightarrow 0$ (Δx

TABLE I. Convergence of the method as $\Delta x \to 0$ ($\Delta r \to 0$) in the calculation of the binding energy $-\varepsilon$ of the ^{11}Be ground state. The ''exact'' results are 0.5013 ($V_0 = -59.5$) and 0.3247 ($V_0 = -58.2$). Energies are in MeV and lengths in fm.

Quasiuniform grid			Uniform grid			
		$-\varepsilon$			$-\varepsilon$	$-\varepsilon$
N_x	Δx	$V_0 = -59.5$	N_r	Δr	$V_0 = -59.5$	$V_0 = -58.2$
125	0.008	0.521	2000	0.4	0.722	0.504
250	0.004	0.506	4000	0.2	0.552	0.365
500	0.002	0.502	8000	0.1	0.514	0.334
			16 000	0.05	0.504	0.327

$\to 0$) by using as a test the calculation of the binding energy of the ^{11}Be ground state. In this case, the eigenvalue problem

$$\hat{H}_0(r)\mathbf{\Psi}(r) = \varepsilon \mathbf{\Psi}(r) \tag{21}$$

is solved with a spherical potential in Eq. (2). For the sake of comparison, the computations are also performed with a uniform grid over r for the two values $V_0 = -59.5$ and -58.2 MeV. The results are compared with ''exact'' energies obtained with the Lagrange-mesh technique [8] with zeros of the $N = 40$ Laguerre polynomial. The analysis shows that the second order finite-difference approximation on a quasiuniform grid with $N_x = 500$ points ($\Delta x = 0.002$), used in the present work, leads to a considerably more accurate value of ε in Eq. (21) than the analogous finite-difference scheme on the uniform grid with $N_r = 2000$ points ($\Delta r = 0.4$ fm). The use of a uniform grid with $\Delta r = 0.4$ fm in Ref. [4] seems to be the main reason for the deviation of their parameter V_0 with respect to ours. Indeed Table I shows that the experimental binding energy is well reproduced for $V_0 = -58.2$ MeV with $\Delta r = 0.4$ fm but that convergence is not reached yet. It is shown in Table I that, for computing the eigenvalue ε on the uniform grid with a 1% accuracy, the number N_r of grid points must be increased at least by a factor of 8 ($\Delta r = 0.05$ fm). The more extended $1/2^-$ excited state is less sensitive to the integration step Δr (or Δx), which explains why the fitted parameter $V_1 = -40.5$ MeV does not deviate much from the value -40.4 MeV used in Ref. [4].

IV. CONVERGENCE OF THE SCHEME

We present an illustration of the convergence of the computational scheme, using as an example a calculation of the mean value $\langle k_z \rangle$ of the longitudinal momentum [3]

$$\langle k_z(t) \rangle = \frac{\int d\boldsymbol{k} k_z |\langle \boldsymbol{k} | \Psi_{\rm bu}(\boldsymbol{r},t) \rangle|^2}{\int d\boldsymbol{k} \langle \boldsymbol{k} | \Psi_{\rm bu}(\boldsymbol{r},t) \rangle|^2} \tag{22}$$

between the neutron emitted in the reaction $^{11}\mathrm{Be} + ^{208}\mathrm{Pb} \to ^{10}\mathrm{Be} + n + ^{208}\mathrm{Pb}$ and the core nucleus ^{10}Be. The notation $|\boldsymbol{k}\rangle$ represents a plane wave. The breakup component is obtained by eliminating the bound states from the calculated wave packet [3,4]

$$|\Psi_{\rm bu}(\boldsymbol{r},t)\rangle = \left(1 - \sum_{\nu \in \text{bound}} |\phi_\nu(\boldsymbol{r})\rangle\langle\phi_\nu(\boldsymbol{r})|\right) |\Psi(\boldsymbol{r},t)\rangle, \tag{23}$$

where the sum runs over the two bound states of ^{11}Be obtained from Eq. (21).

To avoid the slowly convergent and time-consuming three-dimensional integration over the momentum space in Eq. (22), the direct computation in coordinate space

$$\langle k_z(t) \rangle = \frac{\langle \Psi_{\rm bu}(\boldsymbol{r},t) | -i(\partial/\partial z) | \Psi_{\rm bu}(\boldsymbol{r},t) \rangle}{\langle \Psi_{\rm bu}(\boldsymbol{r},t) | \Psi_{\rm bu}(\boldsymbol{r},t) \rangle} \tag{24}$$

has been used instead in Ref. [4]. In the present paper we suggest an alternative approach for the calculation of the mean values $\langle k_z \rangle$ and $\langle k_x \rangle$ through the matrix element of a commutator as in

$$\langle k_z(t) \rangle = i \frac{\mu}{\hbar^2} \frac{\langle \Psi_{\rm bu}(\boldsymbol{r},t) | [\hat{H}(\boldsymbol{r},t), z] | \Psi_{\rm bu}(\boldsymbol{r},t) \rangle}{\langle \Psi_{\rm bu}(\boldsymbol{r},t) | \Psi_{\rm bu}(\boldsymbol{r},t) \rangle}, \tag{25}$$

which avoids the loss of accuracy due to the numerical differentiation over the Cartesian variables in Eq. (24) of the wave packet calculated in spherical coordinates. The calculation is performed, as in the previous theoretical considerations [3,4], according to the bound-neutron model [Eq. (4)] with the straight-line trajectory $\boldsymbol{R}(t) = \boldsymbol{b} + \boldsymbol{v}_0 t$ of the ^{11}Be projectile. The impact parameter is chosen as $b = 12$ fm and the selected relative velocity $v_0 = 0.37c$ corresponds to 72 MeV per nucleon, i.e., the conditions of the experiment [10] as well as the previous calculations [3,4]. The z axis is chosen along $\boldsymbol{v}_0$ and the x axis is in the collision plane.

Since the admixture of the breakup component $\Psi_{\rm bu}(\boldsymbol{r},t)$ in the total wave function $\Psi(\boldsymbol{r},t)$ is only of the order of 10% [4,10], the calculation of the quantity $\langle k_z(t) \rangle$ is a rather challenging computational problem supposed to be very sensitive to variations of the spatial grid parameters N, Δx and r_m, as well as the time grid parameters Δt and $T_{\rm out}$. It provides a good example for analyzing the convergence of the method. Moreover, this analysis is also actual because the previous calculations [3,4] reproduce only half the measured value $\langle k_z \rangle$ of the momentum between the neutron and the core nucleus in the longitudinal direction [10] and the source of this difference has not been clarified so far.

First we analyze the convergence of the method with respect to $N \to \infty$ and the validity of the multipole expansion of operator (4), used in previous calculations [2–4]. We use the quasiuniform grid $\{r_i\}$ fixed above by studying the bound states of ^{11}Be. The value $\langle k_z(t) \rangle$ has been evaluated on a set of successively converging angular grids $\{\Omega_j\}_1^N$ ($N \to \infty$) without and with multipole expansion of operator (4). The initial time was chosen as $T_{\rm in} = -20\hbar$ MeV^{-1}. The results presented in Table II for the average longitudinal momentum show the fast convergence as N increases. For the chosen values of b and v_0, they also indicate a slower convergence with respect to N of the truncated multipole expansions of operator (4) as used in Refs. [2–4]. The accuracy of the dipole+quadrupole ($d+q$) approximation is, however, rather good.

TABLE II. Convergence of the bound-neutron model with a straight-line trajectory as $N\to\infty$ and convergence of the multipole expansion in Eq. (4) for the mean value $-\langle k_z(t)\rangle$ [Eq. (25)] of the longitudinal momentum between the neutron and the core nucleus ($\Delta t=0.02\hbar$ MeV^{-1}, $\Delta x=0.002$, and $r_m=800$ fm). For every N, the values of $\langle k_z(t)\rangle$ obtained without multipole expansion of Eq. (4) are given. For $N=9$ and 25, the values calculated with only the dipole term (d) in a multipole expansion of Eq. (4) and with the dipole and quadrupole terms ($d+q$) are also presented.

t	$N=9$			$N=25$			$N=49$
($\hbar$ MeV^{-1})	d	$d+q$	Eq. (4)	d	$d+q$	Eq. (4)	Eq. (4)
1	0.0171	0.0167	0.0150	0.0171	0.0167	0.0150	0.0150
4	0.0143	0.0120	0.0124	0.0146	0.0124	0.0128	0.0128
7	0.0172	0.0153	0.0154	0.0176	0.0156	0.0158	0.0158
10	0.0136	0.0116	0.0118	0.0140	0.0120	0.0123	0.0123
15	0.0115	0.0097	0.0100	0.0120	0.0102	0.0105	0.0105
20	0.0102	0.0087	0.0090	0.0107	0.0091	0.0094	0.0094

The convergence over $\Delta t\to 0$ is illustrated in Table III as well as the convergence with respect to $\Delta x\to 0$, $r_m\to\infty$, where the values $\langle k_z(t)\rangle$ calculated on a set of successively converging radial $\{r_i\}$ and time $\{t_n\}$ grids are given. The analysis shows that the time grid with $\Delta t=0.02\hbar$ MeV^{-1} gives about a 1% accuracy in calculating the $\langle k_z(t)\rangle$ values for all times in the interval $t\leqslant T_{\rm out}$. However, the radial grid fixed in the previous paragraph by analyzing the energy structure of ^{11}Be ($\Delta x=0.002$, $r_m=800$ fm) gives the same accuracy only for not too large times $t\leqslant 4\hbar$ MeV^{-1}. The presented data show that for getting an asymptotically stable value of $\langle k_z(T_{\rm out})\rangle$ with $T_{\rm out}\simeq 10-20\hbar$ MeV$^{-1}\to\infty$, it is necessary to increase the boundary of integration to $r_m=1200$ fm and to keep the step of integration Δx rather small. In Refs. [3,4], the boundaries of integration were chosen as $r_m=800$ fm and $T_{\rm out}=-T_{\rm in}=10\hbar$ MeV^{-1}.

The calculated values $\langle k_z\rangle=-0.0157$ fm^{-1} and $\langle k_x\rangle=0.0480$ fm^{-1} at $T_{\rm out}=10\hbar$ MeV^{-1} can be compared with the previous results $\langle k_\parallel\rangle=-0.019$ and $\langle k_\perp\rangle=0.052$ fm^{-1} obtained in Ref. [4]. The difference between our results and the previous ones can be explained by the use of a more detailed radial grid and by the avoidance of a multipole expansion of the operator (4) in the present calculations (see Tables I, II, and III).

V. RESULTS AND DISCUSSION

With the developed model, we now analyze the dependence of the mean transverse and longitudinal momenta of the emitted neutron, on postacceleration effects. In Fig. 2, the calculated values $\langle k_z(t)\rangle$ and $\langle k_x(t)\rangle$ are given as a function of time. The transverse momentum $\langle k_x\rangle$ has been evaluated with a formula analogous to Eq. (25).

A set of calculations have been done with different choices of the time-dependent Coulomb interaction $V_C(\boldsymbol{r},t)$ in Eq. (3). First we have considered a bound-neutron model (4) with a straight-line trajectory (i.e., without any deceleration or acceleration of the projectile).

Then the model has been improved by considering in Eq. (4) a Coulomb trajectory. As one can see from the figures, the correction of the trajectory $\boldsymbol{R}(t)$ weakly influences the values of $\langle k_x\rangle$ and slightly more the values of $\langle k_z\rangle$. However, estimating the effects of postacceleration is possible through a comparison with the free-neutron model according to Eq. (5) (i.e., assuming that the freedom of the neutron occurring after the breakup is realized during the full reaction process). The average momentum $\langle k_x\rangle$ changes considerably, in agreement with the simple classical modeling of the ''free particle'' mechanism [11]. The $\langle k_z\rangle$ evaluated with the free-neutron model becomes closer to the experimental one, but

TABLE III. Illustration of the method convergence as $\Delta t\to 0$ and $\Delta x\to 0$, $r_m\to\infty$ for the mean value $-\langle k_z(t)\rangle$ [Eq. (25)] of the longitudinal momentum between the neutron and the core nucleus ($\Delta t_0=0.02\hbar$ MeV^{-1}).

t	$r_m=800$ fm $\Delta x=0.002$	$r_m=800$ fm $\Delta x=0.002$	$r_m=1200$ fm $\Delta x=0.0005$	$r_m=1200$ fm $\Delta x=0.0004$	$r_m=1500$ fm $\Delta x=0.0004$
($\hbar$ MeV^{-1})	$\Delta t=\Delta t_0$	$\Delta t=\frac{1}{2}\Delta t_0$	$\Delta t=\Delta t_0$	$\Delta t=\Delta t_0$	$\Delta t=\Delta t_0$
1	0.0150	0.0147	0.0150	0.0150	0.0150
4	0.0128	0.0129	0.0134	0.0134	0.0134
7	0.0158	0.0157	0.0176	0.0176	0.0176
10	0.0123	0.0122	0.0156	0.0157	0.0157
15	0.0105	0.0103	0.0159	0.0161	0.0161
20	0.0094	0.0092	0.0158	0.0162	0.0162
25			0.0154	0.0160	0.0162
30			0.0148	0.0156	0.0157

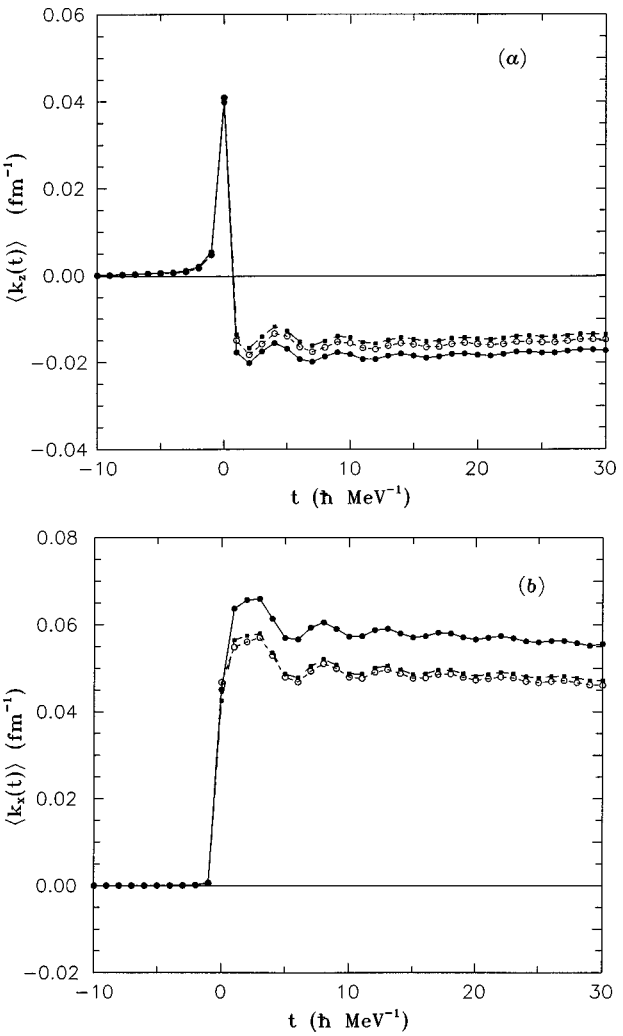

FIG. 2. Time dependence of the mean longitudinal $\langle k_z(t)\rangle$ (a) and transverse $\langle k_x(t)\rangle$ (b) momenta. The calculations are performed on the grid $N=25$, $\Delta x=0.0005$, $r_m=1200$ fm, $\Delta t=0.01\hbar$ MeV^{-1}, $T_{\rm in}=-20\hbar$ MeV^{-1}. Open circles correspond to the data obtained with the bound-neutron model (4) with a straight-line trajectory. Calculations with a Coulomb trajectory $\boldsymbol{R}(t)$ in potential (4) are indicated by full squares. Calculations with the free-neutron model (5) are displayed as full circles.

the considerable difference of about a factor of 2 between the calculated and experimental values remains.

The developed method has also been applied to the total breakup cross section. We have calculated this cross section as a function of the energy E of the relative motion between the emitted neutron and the core nucleus by the formula

$$\frac{d\sigma_{\rm bu}(E)}{dE} = \frac{4\mu k}{\hbar^2}\int_{b_{\rm min}}^{b_{\rm max}}\sum_{lm}\left|\int j_l(kr)Y_{lm}(\hat{\boldsymbol{r}})\Psi_{\rm bu}(\boldsymbol{r},T_{\rm out})d\boldsymbol{r}\right|^2 bdb. \tag{26}$$

Again we first apply the bound-neutron model with the straight-line $\boldsymbol{R}(t)$ trajectory in the time-dependent Coulomb potential (4), as in the previous calculations [2–4]. Then corrections due to the projectile deflection from the straight-line trajectory and postacceleration effect are evaluated.

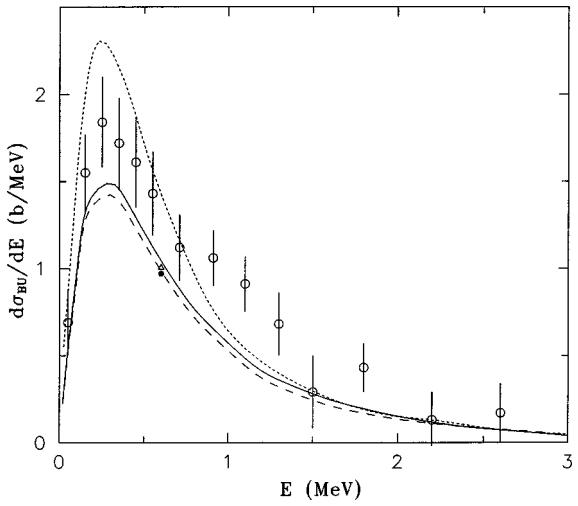

FIG. 3. Total breakup cross sections $d\sigma_{\rm bu}(E)/dE$. Calculations are performed with the bound-neutron model (4) with a straight-line trajectory on the $N=25$ angular grid for $\Delta t=0.01\hbar$ MeV^{-1} and $T_{\rm out}=-T_{\rm in}=20\hbar$ MeV^{-1}. The dashed line represents the results obtained on the quasiuniform grid $\Delta x=0.002$, $r_m=800$ fm. The solid line shows the results from the grid $\Delta x=0.0005$, $r_m=1200$ fm. The triangle indicates the result obtained with a Coulomb trajectory $\boldsymbol{R}(t)$ in potential (4) and the full circle indicates the result of the free-neutron model (5) ($\Delta x=0.0005$, $r_m=1200$ fm). The boundaries of integration over b are chosen as $b_{\rm min}=12$ fm and $b_{\rm max}=400$ fm. The previous (partly perturbative) results of Ref. [4] are represented as a dotted line. The experimental data are from Ref. [10].

The calculated total breakup cross sections are displayed in Fig. 3 together with the experimental data [10] and the most accurate previous theoretical results [4]. One can see that the previous calculation essentially overestimates the breakup cross section near the maximum as compared with the present results and the experimental data (see Fig. 3). In previous works [3,4], a simplified bound-neutron model with a straight-line trajectory of the projectile has been used. Specifically the multipole approximation of the time-dependent Coulomb potential (4) and a less detailed grid were used in Ref. [4]. The previous calculations were also partly perturbative, i.e., integral (26) was calculated numerically on the interval [$b_{\rm min}=12$ fm, $b_{\rm max}=30$ fm] and the remaining part was evaluated with the first-order perturbation theory. In the present calculation, this integral is calculated numerically over the whole interval [$b_{\rm min}=12$ fm, $b_{\rm max}=400$ fm]. Our analysis shows that using more accurate spatial and time grids as well as avoiding the multipole approximation gives an effect of the order of a few percents near the maximum of the breakup cross section. The main part of these corrections, due to the extension of the boundary of integration over the radial variable from the value $r_m=800$ fm used in Ref. [4] to $r_m=1200$ fm, is illustrated in Fig. 3. Therefore the use of the first-order perturbation theory in Ref. [4] for evaluating the main part of the integral (26) on the interval [$b_{\rm max}=30$ fm, ∞] may be the main source leading to the overestimation of the breakup cross section near the maximum as compared with our results and the experimental data (see Fig. 3). Table IV illustrates the convergence of the integral

TABLE IV. Convergence of the method for the breakup cross section $d\sigma(E,b_{\max})/dE$ (in b/MeV) as a function of the impact parameter $b_{\max}$ (in fm) and the energy E (in MeV). The calculation is performed with $N=25$, $\Delta x=0.002$, $r_m=800$ fm, and $\Delta t=0.01\hbar$ MeV^{-1} over the time interval from $T_{\rm in}=-20\hbar$ MeV^{-1} to $T_{\rm out}=20\hbar$ MeV^{-1}.

$b_{\max}$	$E=0.2$	$E=0.3$	$E=0.6$	$E=1.2$	$E=2.0$	$E=2.8$
12	0.036	0.043	0.044	0.024	0.011	0.006
30	0.543	0.618	0.526	0.242	0.102	0.051
50	0.856	0.948	0.755	0.322	0.126	0.060
100	1.196	1.279	0.938	0.364	0.134	0.062
200	1.349	1.407	0.982	0.369	0.134	0.062
300	1.369	1.421	0.985	0.369	0.134	0.062
400	1.373	1.423	0.985	0.369	0.134	0.062

(26) as a function of the upper bound $b_{\max}$ for a few energies E for the same boundary of integration r_m over the radial variable as in Ref. [4]. It shows that the integration over the interval [30 fm, 400 fm] gives about 60% of the calculated cross section near the maximum. Thus inaccuracies of the first-order perturbation theory may therefore significantly reduce the global accuracy of the results. A possible source for the loss of accuracy may be the time propagation on a not detailed enough radial grid for the wave function in the perturbative term (16) of Ref. [4]. Actually, as shown in Sec. III, the radial grid used in Ref. [4] gives a noticeably less accurate description of the ^{11}Be ground state than our scheme.

Corrections due to the projectile deflection from the straight-line trajectory and postacceleration effect are found to be weak (see Fig. 3) and do not destroy the rather good agreement of the calculated cross sections with the experimental ones.

We also examined the effect of the neutron spin coupling with the varying field of the target determined by Eq. (6). For the considered values of impact parameters and colliding energies, it does not exceed the order of 0.2% in the values of $\langle k_x\rangle$, $\langle k_z\rangle$, and $d\sigma_{\rm bu}(E)/dE$ and can be neglected.

Note that including the small impact parameters from the interval $[0,b_{\min}=12$ fm] in the computational scheme should increase the total cross sections and lead to a better agreement with the experimental data. However, estimates of this part of the integral (26) demands correcting the time-dependent Coulomb interaction (4) by nuclear effects at $b<12$ fm.

In conclusion of the discussion of the total breakup cross section, we mention two recent calculations [12,13], giving values closer to our results and experimental data [10] than to those of Ref. [4]. The first work [12] applies a semiclassical coupled-channel scheme with a wave function expansion over a stationary basis. The basis includes bound and low-lying states of the discretized continuum for the first three partial waves. The introduction of the nuclear interaction with a nucleus-nucleus optical potential avoids the need for a cutoff over the impact parameter b. This analysis suggests a cutoff in impact parameter at about 11.5 fm, close to our $b_{\min}=12$ fm used in Refs. [3,4,10]. Unlike our results, these calculations are partly perturbative due to the multipole expansion for the interaction potential. In Ref. [13] a quantal nonperturbative but stationary computational scheme has been applied.

VI. CONCLUSION

In this work, we suggested a nonperturbative time-dependent approach for the quantitative analysis of the Coulomb breakup of halo nuclei. By using as an example the $^{11}\mathrm{Be}+^{208}\mathrm{Pb}\rightarrow{}^{10}\mathrm{Be}+n+^{208}\mathrm{Pb}$ breakup reaction, we illustrated the fast convergence of the method and its efficiency.

The suggested three-dimensional mesh approximation possesses the advantage that a local interaction is diagonal in such a representation. As a consequence, it allows avoiding the use of the multipole expansion of the time-dependent Coulomb interaction between the projectile and the target as well as the straight-line approximation for the projectile trajectory used in the previous calculations. Postacceleration effects may be treated in a natural way in such an approach by using other types of trajectories.

The splitting-up method only requires a simple diagonalization procedure for the remaining nondiagonal part of the kinetic energy operator. It gives a fast convergence with respect to the numbers of grid points (N and N_x). The computational time is directly proportional to the numbers N and N_x. It allowed us to extend the boundaries of integration over the radial and time variables. It also permits avoiding the perturbative approximations used in Refs. [3,4] for evaluating the breakup cross sections.

These advantages make the method promising for applications to other breakup reactions, particularly with emission of a proton (see, for example, Ref. [14]). Another interesting, but more difficult application may be breakup reactions with two-neutron halo nuclei.

The effect of the neutron postacceleration in the breakup of ^{11}Be has also been investigated in this approach by comparing the results obtained with two different Coulomb trajectories followed by the full halo nucleus and by its core. Including their effect slightly improves the mean values of the transverse momentum of the emitted neutron.

The present model could easily deal with nuclear effects between target and projectile occurring at lower energies and/or at smaller impact parameters. The only minor modification would be using the complex values of the optical potentials between target and projectile or projectile fragments (see, for example, Ref. [12]).

ACKNOWLEDGMENTS

V.S.M. would like to thank Drs. F.M. Penkov and V.A. Kuzmin for many useful discussions and suggestions and the staff of the P.N.T.P.M. of the Free University of Brussels for warm hospitality. He also gratefully acknowledges the warm hospitality and the use of the computer resources of IMEP of the Austrian Academy of Sciences. This text presents research results of the Belgian program on interuniversity attraction poles initiated by the Belgian-state Federal Services for Scientific, Technical and Cultural Affairs. V.S.M. was partly supported by that program.

[1] I. Tanihata, J. Phys. G **22**, 157 (1996).
[2] H. Esbensen, G. F. Bertsch, and C. A. Bertulani, Nucl. Phys. **A581**, 107 (1995).
[3] T. Kido, K. Yabana, and Y. Suzuki, Phys. Rev. C **50**, R1276 (1994).
[4] T. Kido, K. Yabana, and Y. Suzuki, Phys. Rev. C **53**, 2296 (1996).
[5] V. S. Melezhik, Hyperfine Interact. **101/102**, 365 (1996).
[6] V. S. Melezhik, Phys. Lett. A **230**, 203 (1997).
[7] V. S. Melezhik, in *Atoms and Molecules in Strong External Fields*, edited by P. Schmelcher and W. Schweizer (Plenum, New York, 1998), p. 89.
[8] D. Baye, J. Phys. B **28**, 4399 (1995).
[9] G. I. Marchuk, in *Partial Differential Equations. II. SYNSPADE-1970* (Academic, New York, 1971).
[10] T. Nakamura, S. Shimoura, T. Kobayashi, T. Teranishi, K. Abe, N. Aoi, Y. Doki, M. Fujimaki, N. Inabe, N. Iwasa, K. Katori, T. Kubo, H. Okuno, T. Suzuki, I. Tanihata, Y. Watanabe, A. Yoshida, and M. Ishihara, Phys. Lett. B **331**, 296 (1994).
[11] G. F. Bertsch and C. A. Bertulani, Nucl. Phys. **A556**, 136 (1993).
[12] C. H. Dasso, S. M. Lenzi, and A. Vitturi, Phys. Rev. C **59**, 539 (1999).
[13] P. Banerjee, I. J. Thompson, and J. A. Tostevin, Phys. Rev. C **58**, 1042 (1998).
[14] F. Negoita, C. Borcea, F. Carstoiu, M. Lewitowicz, M. G. Saint-Laurent, R. Anne, D. Bazin, J. M. Corre, P. Roussel-Chomaz, V. Borrel, D. Guillemaud-Mueller, H. Keller, A. C. Mueller, F. Pougheon, O. Sorlin, S. Lukyanov, Y. Penionzhkevich, A. Fomichev, N. Skobelev, O. Tarasov, Z. Dlouhy, and A. Kordyasz, Phys. Rev. C **54**, 1787 (1996).